https://doi.org/10.15407/ufm.26.03.598

V.A. DEKHTYARENKO 1,2,*, V.K. NOSENKO 1,**, V.V. KYRYLCHUK 1,***, A.V. NOSENKO 1,****, O.M. SEMYRGA 1,*****, I.K. YEVLASH 1, and V.I. BONDARCHUK 1

- ¹G.V. Kurdyumov Institute for Metal Physics of the N.A.S. of Ukraine, 36 Academician Vernadsky Blvd., UA-03142 Kyiv, Ukraine
- ² E.O. Paton Electric Welding Institute of the N.A.S. of Ukraine, 11 Kazymyr Malevych Str., UA-03150 Kyiv, Ukraine
- *devova@i.ua, ** victorn58@ukr.net, *** kyrylchuk_v@ukr.net, **** itrij@ukr.net, ***** o semyrga@ukr.net

AMORPHOUS ALLOYS AS A PROMISING CLASS OF FUNCTIONAL MATERIALS. Pt. 1: Manufacturing Methods, Structure, Physical and Mechanical Properties

The paper considers a special class of structural materialssamorphous alloys. Unlike crystalline alloys, there is no translation symmetry in the arrangement of atoms in amorphous alloys, which have only short-range atomic order. As demonstrated, the primary experimental techniques for confirming the formation of an amorphous structure are X-ray diffraction analysis (XRD) and differential scanning calorimetry (DSC). The effects of the manufacturing processes, structural relaxation, and solidification on the mechanical properties of amorphous alloys are discussed. The differences in the deformation processes between crystalline and amorphous alloys are considered. Deformation of crystalline alloys occurs due to dislocation sliding, whereas amorphous alloys are deformed due to the local rearrangement of atoms that requires significantly higher energies or stresses. As shown, three main types of crystallisation processes can occur, depending on the chemical composition of an amorphous alloy. The first one is polymorphic crystallization, when an amorphous alloy is transformed into a supersaturated solid solution, a metastable or stable crystalline phase without changing its

Citation: V.A. Dekhtyarenko, V.K. Nosenko, V.V. Kyrylchuk, A.V. Nosenko, O.M. Semyrga, I.K. Yevlash, and V.I. Bondarchuk, Amorphous Alloys as a Promising Class of Functional Materials. Pt. 1: Manufacturing Methods, Structure, Physical and Mechanical Properties, *Progress in Physics of Metals*, 26, No. 3: 598–625 (2025)

© Publisher PH "Akademperiodyka" of the NAS of Ukraine, 2025. This is an open access article under the CC BY-ND license (https://creativecommons.org/licenses/by-

nd/4.0)

composition. In the second case, two crystalline phases are formed simultaneously due to the eutectic reaction. The third type corresponds to primary crystallization, when stable or metastable phase is formed at the first stage.

Keywords: amorphous alloy, metallic glass, cooling rate, short-range atomic order, mechanical properties.

1. Main Techniques for Manufacturing Amorphous Metal Alloys (AMAs)

For the first time, amorphous alloys were manufactured by quenching from vapour and electrodeposition in the 50s of the last century [1], and in 1960, Klement and co-authors reported that they produced amorphous metal by quenching from melt [2]. Even today, the issue of manufacturing amorphous materials remains relevant [3–7]. According to Ref. [8], the progress of science is always closely linked to technological breakthroughs, and this applies to the metallic glass production (Fig. 1).

One of the most promising ways to produce metal alloys in a metastable state with various deviations from equilibrium, up to those with a noncrystalline structure, is ultra-rapid cooling (URC) of the melt. The supercooling necessary to prevent nucleation and growth of crystallites is achieved by very rapid cooling of the melt: $V_{\rm cool}^{\rm cr}$ (critical cooling rate) is about from 10^{10} to 10^{12} K/s for pure metals, and 10^6 K/s for metal alloys [9].

Metal glass is mainly produced by cooling the melt at a relatively high rate to avoid crystallization during solidification [8]. Therefore, from a structural viewpoint, metallic glasses are often considered as frozen metallic liquids. The process of melt quenching and conditions of glass formation are schematically shown in the time-temperature-transformation (TTT) diagram (Fig. 2). According to it, cooling rates of the order of $\cong 10^5-10^6$ K/s are usually needed to form fully amorphous structures in binary alloy systems. Simply put, the atoms in the melt do not have enough time to arrange into a crystal lattice under these conditions, so the disordered atomic structure of the melt is preserved at lower temperatures.

Various URC techniques developed to date are distinguished by the method of forming the liquid metal in contact with the heat sink (discretesdispersion or local melting, or continuousscasting), by the type of cooling medium (gas, liquid, or solid) and location of this medium (single, double or multilateral cooling). These techniques make it possible to produce rapid-quenched materials in the form of films, powders, fibres, ribbons, chips or coatings, *i.e.*, objects that are small at least in one linear dimension [10, 11]. Besides, there is a separate, relatively new class of materials: bulk metal glasses (BMGs) [12, 13].

The most common technique to produce rapid-quenched, in particular amorphous, materials is cooling of a continuous melt jet on the outer surface of a rotating disk, the so-called melt spinning (Chill Block Melt Spinning, or CBMS) [14].

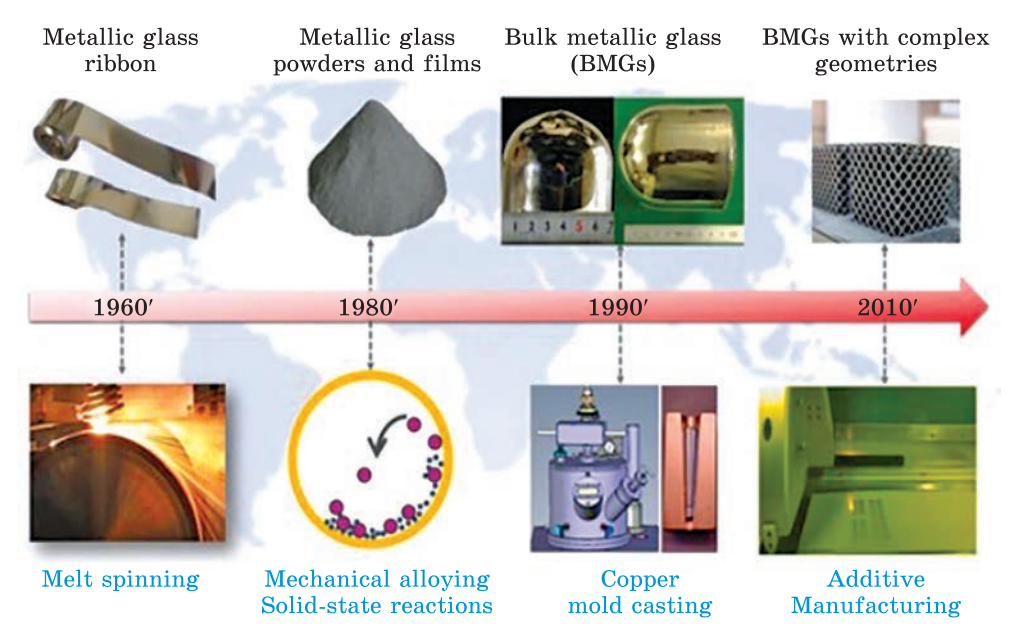


Fig. 1. The development of MG and BMG research is largely associated with advances in their manufacturing techniques [8]



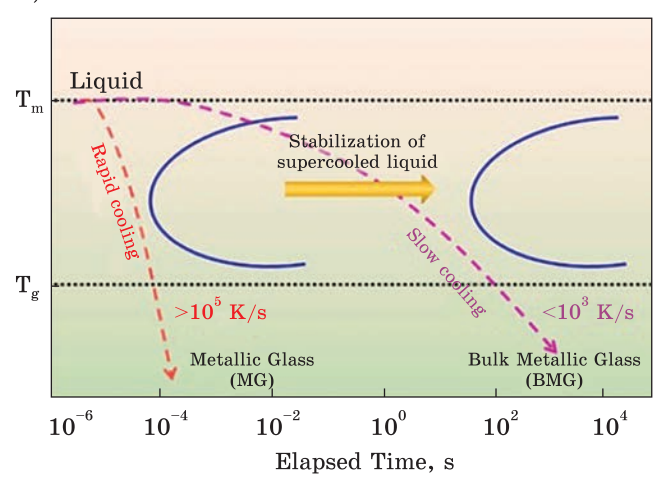


Fig. 2. Time-temperature transformation (TTT) curves for formation of metallic glasses (MGs) and bulk metallic glasses (BMGs) [8]

The main feature of this technique is the ability to form a continuous ribbon whose width is determined only by technological parameters, and high productivity. The maximum

There are two types of the above technique, which differ in the way, in which the melt is fed to the surface of the quenching disk: cylindrical free jet (free jet melt spinning—FJMS), and planar flow (planar flow casting—PFC) with a significantly reduced distance between the nozzle edge and cooling surface. The maximum width of the tape in the former case does not exceed ≈5 mm, whereas in the latter case, it has no fundamental

limitations. The geometry, structure and other characteristics of the re-

achievable cooling rate during melt spinning is estimated as 10⁶ K/s [14].

sulting ribbons are determined by the spinning parameters. The most important parameters are the following: melt temperature; jet shape, cross section, incidence angle and speed; material, temperature, spinning speed and surface condition of the cooling disk; distance between the nozzle and the cooling surface; composition and pressure of the ambient gas environment [15].

An increase in the melt temperature before pouring $T_{\rm p}$ can affect cooling rate $V_{\rm cool}$ in different ways: on the one hand, overheating of the melt somewhat reduces this rate due to local heating of the cooling surface (a difference in $T_{\rm p}$ by 100 K changes $V_{\rm cool}$ by 5–7% [16]); on the other hand, the melt spreads into a thinner ribbon due to lower viscosity and surface tension, which leads to an increase in $V_{\rm cool}$. According to Ref. [14], a relatively high melt viscosity before casting contributes to the production of thicker amorphous ribbons of improved quality, but there is no consensus on the value of optimal melt overheating before casting [14].

2. Features of Structure, Physical and Mechanical Properties of AMAs

The structural state of amorphous metal alloys, unlike crystalline ones, is characterized by the absence of translation symmetry in the arrangement of atoms, and the presence of only the short-range atomic order [17]. However, the authors of Ref. [18] note that despite amorphous alloys having a disordered atomic structure, it is difficult to determine their electronic structure; a large amount of experimental research has shown that their non-periodic structure is not completely random. Some clear signs of atomic layering are observed already at the distance of the third closest neighbour.

According to the literature [19], X-ray phase analysis (XRD) and differential scanning calorimetry (DSC) are most often used to reveal an amorphous structure (Fig. 3). When XRD technique is used, the presence of a broad diffuse (halo-type) peak without sharp peaks is often considered evidence of the presence of an amorphous/glassy phase (Fig. 3, a). This peak can shift to smaller or larger angles, depending on the average distance of the first neighbour atom in a random arrangement of atoms. A DSC curve for an amorphous/glassy alloy allows measuring such thermal parameters as T_g , T_x , and DT_x . In the DSC curve of a typical glassy alloy shown in Fig. 3, b, the supercooled liquid region with endothermic reaction first appears when heating from the room temperature. The temperature of starting this endothermic reaction corresponds to the glass-transition temperature T_g . With further heating, crystallization occurs with a large exothermic peak; the temperature of the exothermic peak onset corresponds to the crystallization temperature T_x .

It should also be noted that, according to Ref. [19], there is a difference in the behaviour between crystalline, amorphous, and glassy alloys

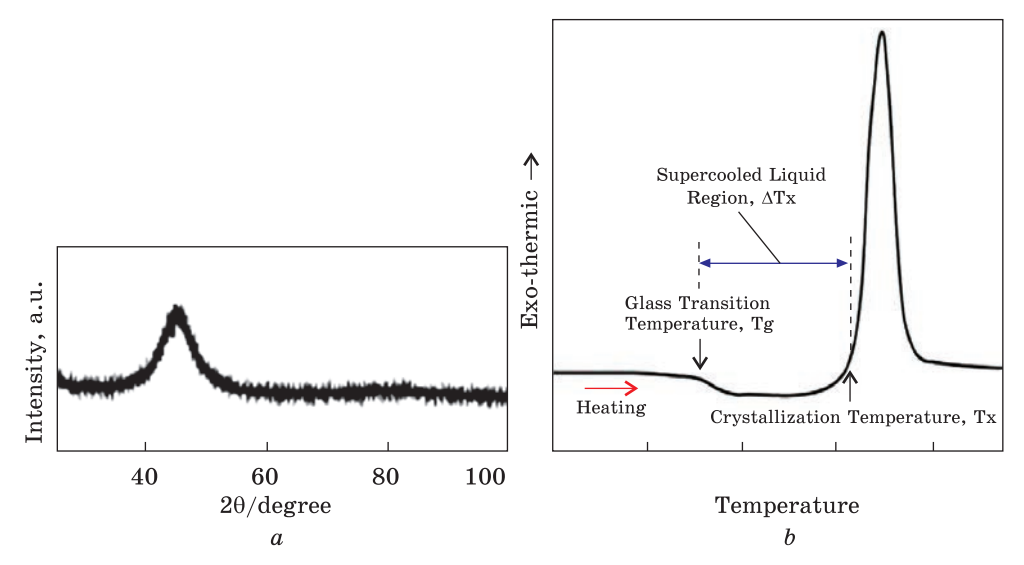


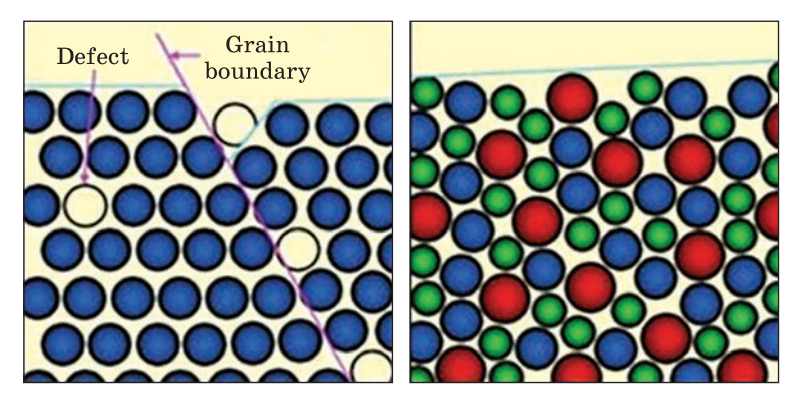
Fig. 3. Typical X-ray diffraction pattern (a) [20] and DSC curve (b) [19] for amorphous alloy

during transformations upon heating. In the temperature range from room temperature to the melting point T_m , the following transformations occur: only melting for a crystalline alloy; in an amorphous alloy, first, the transition to the crystalline state at the crystallization temperature T_x (Fig. 3, b), and then, melting at T_m ; in a metallic glass, first, the transition into the supercooled liquid state at the glass-transition temperature T_g (Fig. 3, b), then, crystallization at T_x , and finally melting at T_m . The amorphous alloys and metallic glasses are distinguished by the transition into the supercooled liquid state, which is inherent in metallic glasses.

In the case of multicomponent systems, the concept of short-range order includes not only the spatial arrangement of atoms regardless of their sort (topological or configurational short-range order), but also the ordered arrangement of atoms of different types, *i.e.*, chemical or compositional short-range order.

The short-range atomic order in AMAs is geometrically represented using various models, which are covered in detail in the literature [21–24].

The criterion for the applicability of a particular model is usually good agreement between calculated and experimental values of radial distribution functions (RDFs) of atoms. Since this condition is necessary, but not sufficient for unambiguous conclusions about the adequacy of the model to describe the real structure, there are various models of the AMA structures (e.g., random close packing of spheres [25, 26], microcrystalline [27], cluster [28, 29], polycluster [30], relaxation [31], and others), which have different degrees of approximation of certain parameters to the real structures.



Lattice Structure

Random Atom Arrangement

Fig. 4. Schematic illustrations of atom arrangements in a crystalline alloy and an amorphous/glassy alloy with their structural features [19]

Most of the experimental results on the atomic structure of AMAs can be explained within the framework of the concepts of the existence of structural and concentration inhomogeneities, the formation of atomic nanogroups that differ in packing types and the ratio of atoms of different types.

For two-component amorphous Fe-B alloys, A.V. Romanova *et al.* [32, 33] showed that the short-range atomic order is well described by a two-structure model, according to which there are microgroups of two types with different topological and compositional short-range order. The main type that determines the parameters of the structural factor and RDF is microgroups (clusters) of Fe atoms with a low content of B atoms and with close packing. In other clusters, B atoms have an ordered arrangement relative to Fe atoms, and the concentration of the former atoms is much higher than the average one for the alloy; these clusters are characterized by a strong interaction of atoms of different types, which is typical for borides (chemical short-range order) [33].

Direct evidence for the existence of clusters of these two types was obtained due to the study of the microstructure of amorphous $Fe_{84}B_{16}$ alloy [34], as well as due to neutron diffraction studies of $Fe_{83}B_{17}$ alloy [35].

As shown in Ref. [32], the atomic structure of amorphous alloys, in particular Fe-B and others, is very similar to the structure of melts of the corresponding concentrations, and this is an additional argument in favour of the fact that the amorphous state can be considered as a superviscous melt.

As mentioned above, amorphous alloys have a random arrangement of atoms, similar to a liquid, so their properties are fundamentally different from those of crystalline alloys. Figure 4 shows the arrangement of atoms in crystalline alloy and amorphous alloy/metallic glass [19].

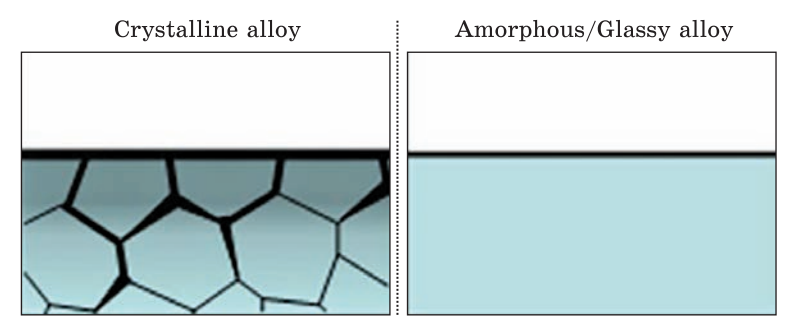


Fig. 5. Comparison of corrosion resistivity of crystalline alloy and amorphous/glassy alloy [19]

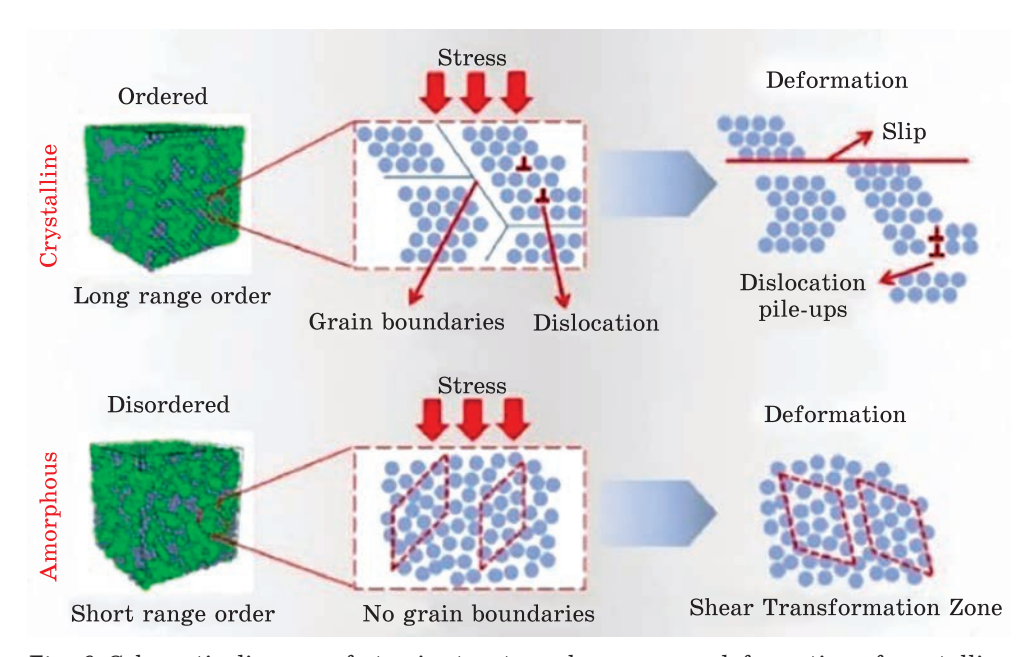


Fig. 6. Schematic diagram of atomic structure changes upon deformation of crystalline and amorphous solids under stress [41]

As seen in Fig. 4, a conventional crystalline alloy has a crystal lattice and is polycrystalline with a lot of grains and defects such as grain boundaries, segregations, vacancies, dislocations, etc. Due to a crystal lattice and microstructure, crystalline alloys have high electrical conductivity, high thermal conductivity, they are plastically deformable. On the other hand, amorphous alloys have a random arrangement of atoms similar to liquids, without a crystal lattice and grains. The electrical conductivity of amorphous alloys is an order of magnitude lower than that of crystalline alloys due to the random arrangement of atoms, which prevents the free movement of electrons. However, amorphous alloys have outstanding me-

chanical, electrochemical and magnetic properties due to the absence of dislocations and grain boundaries [36, 37]. In particular, AMAs have high strength (yield strength up to 4500 MPa) and hardness (HV=3.2 UTS) [38] combined with sufficient ductility and abrasive wear resistance [39]. According to Ref. [36], the disordered structure of AMAs causes the following properties: high specific electrical resistance at low, and even sometimes negative (in °C), temperatures and thermal coefficient; high magnetic permeability; low coercive force (of about 0.01 A/m).

Almost all AMAs have high corrosion resistance in aggressive environments (Fig. 5), and some of them (e.g., Fe-based AMAs [40]) have high catalytic activity in various types of chemical reactions [39].

According to Ref. [19], since amorphous alloys and metallic glasses have a random arrangement of atoms, they are unstable (non-equilibrium) and have higher internal energy as compared to crystalline alloys. Therefore, amorphous alloys and metal glasses can corrode in an aggressive environment at the initial stages of the corrosion process. Nevertheless, a new passive surface film forms after the surface layer dissolves. Amorphous alloys and metallic glasses do not contain any defects such as grain boundaries, dislocations and second-phase inclusions; so, this newly formed passive surface film is very homogeneous and protective. That is why they have high corrosion resistance (see Fig. 5).

The differences in deformation processes in crystalline and amorphous alloys were discussed in Refs. [18, 41] (Fig. 6). The deformation of crystalline alloys occurs due to dislocation sliding, whereas amorphous alloys deform due to local atomic rearrangements. Therefore, the deformation of amorphous alloys requires significantly higher energies or stresses as compared to crystalline ones.

3. Relaxation of the Atomic Structure of Amorphous Alloys during Heating

Heating of amorphous alloys to temperatures below T_x increases the mobility of atoms, which tend to transit to more energetically favourable states. The transition of atoms to more equilibrium configurational states is considered structural relaxation (SR) [42]. Therefore, structural relaxation is not the initial stage of crystallization, but is a process that leads to a more stable amorphous state.

Homogeneous relaxation, more commonly called structural relaxation, occurs homogeneously throughout the sample and preserves amorphous structure. During SR, the short-range order changes, which are usually accompanied by only a slight decrease in glass disequilibrium. Unstable atomic configurations arising at the moment of amorphization during the quenching transform into stable configurations due to small displacements of atoms. As a result, the amorphous matrix becomes more compact due to

partial annihilation and removal of excess free volume. It is essential that the displacements of atoms during structural relaxation are smaller than the interatomic distances, and these displacements occur in local zones. The SR process changes a number of physical properties of amorphous alloys [43]: heat capacity, density, electrical resistance, internal friction, elastic properties, hardness, corrosion resistance, magnetic characteristics (Curie temperature changes and magnetic anisotropy appears), etc.

Some models have been proposed to describe SR, which can be divided into two groups: (i) AES (activation energy spectrum) models; (ii) the model of van den Beukel *et al*.

The first model assumes that SR is caused by local rearrangements of atoms in an amorphous material, which occur with different relaxation times (activation energies). The basics of the model were applied [44–46] to relaxation processes in glasses. It is assumed that the distribution of activation energies of these processes has a continuous smooth spectrum. The rate of change of a physical property is proportional to the rate of change of the density of 'kinetic processes'.

The second model [47, 48] uses the approach to describing SR based on the short-range order classification proposed by T. Egami [49]. It is assumed that compositional (chemical) short-range ordering occurs at the first stage of relaxation. This contribution is well described by the AES model and is a reversible process that has the activation energy spectrum from 150 to 250 kJ/mol. Chemical ordering is quite transient, and after its completion, topological short-range ordering becomes decisive. Chemical ordering is a rather fast process; after its completion, topological short-range order becomes a determining factor.

The topological relaxation is described by the free volume model of F. Spaepen [50–52] with activation energy of about 250 kJ/mole; it is an irreversible process. It should be emphasized that, according to the basic idea of Spaepen's model, the heterogeneity of the glass structure causes the formation of zones with excess free volume relative to the 'ideal structure', which act as 'relaxation centres'. In these zones, thermally activated motion of atoms is possible, which causes redistribution of the free volume inside the material, as well as its partial migration to the free surface.

Besides the abovementioned ones, models of the activation energy spectrum are also frequently used. The model of directed structural relaxation, *i.e.*, relaxation driven by external stress, is considered the most promising [53, 54].

Nevertheless, changes in most physical properties of AMAs during annealing have been studied in detail and described both within the model of 'topological and chemical ordering' proposed by van den Beukel [55–57], and within the model of the activation energy spectrum [58, 59].

4. Free Volume and Annealing Embrittlement

A characteristic structural feature of all amorphous alloys is the presence of free volume (FV), since the density of an alloy in the amorphous state is always lower as compared to the crystalline state. The free volume model can provide a fairly clear picture of all stages of structural relaxation and the mechanism of plastic deformation of AMAs [60]. The authors note that free volumes (FVs) are low-density zones, which have a certain size distribution (from fractions of an atomic diameter to hundreds of nanometres). FV size depends on the manufacturing conditions, composition, heat treatment and a number of other factors. Within the framework of this model, it is possible to trace experimentally the evolution of FV zones, starting from their origin in low-density regions in the melt by transforming their shape and redistribution across the thickness of the amorphous ribbon during melt quenching, and ending with changes in the morphology and size distribution of these defects under various external impacts. It should be noted that, given the continuous distribution of sizes of the FV zones, different fractions of these defects have significantly different activation energies and migration mechanisms.

Let us briefly discuss the experimental evidence for the presence of free volume in AMAs. As known [61], the density of an AMA is several percent lower than that of crystalline alloys of the same chemical composition. At the stage of structural relaxation, the amorphous matrix is compacted due to the partial vanishing (annihilation) and removal of excessive FV.

Small-angle X-ray scattering experiments revealed in amorphous alloys regions with electron density fluctuations ranging from several nanometres to several hundred nanometres [62]. The parameters of these regions changed under the impact of surfactants, as well as during structural relaxation processes, which allows suggesting that the free volume zones are the main scattering centres. It was also found [62] that these zones play an important role in the formation of microcracks under mechanical stresses.

There are nanosized and submicroscopic pores corresponding to the free volume zones of a certain fraction [60]. The volume density of submicroscopic pores increases especially at the stage of fixed dilatometric compaction, when FV most intensively migrates from the amorphous matrix not only to the outer but also to the inner free surfaces.

In the study of submicroscopic crystalline Fe-based alloys produced by quenching from the liquid state, a very high density of prismatic dislocation loops and submicroscopic pores ($10^{10}-10^{11}$ mm⁻³) was observed [60]. The only difference between rapidly quenched crystalline alloys and the amorphous ones is that the volume density of FV in the amorphous state is two orders of magnitude higher than that in the crystalline one.

In general, FVs can be divided into excessive and structurally determined. Removal of excessive FVs does not change the symmetry and topological characteristics of the amorphous state. This most mobile component of free volume is responsible for the changes in the structure, physical and mechanical properties of amorphous alloys at the SR stage [63]. The structurally determined free volume is an element of the structure, a part of atomic complexes that determine the topological and compositional characteristics of the amorphous state.

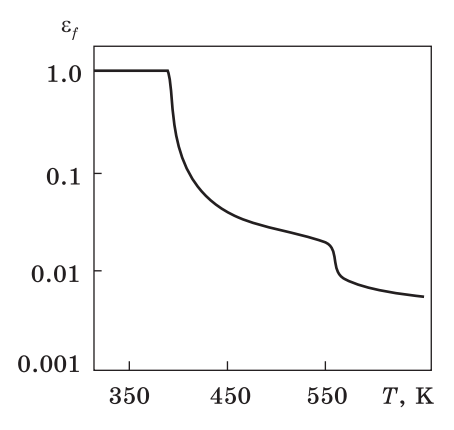
In Ref. [64], the shape of the free volume zones and the features of their distribution in cross cross-section of amorphous ribbons were determined through small-angle X-ray scattering (SAXS). The interpretation of SAXS data still does not look unambiguous, since several sources of scattering are possible: microscopic discontinuities, particles of other phases, zones enriched with an alloying element or those with an increased level of internal stresses. In this regard, a physical parameter of external impact was introduced, which permitted unambiguously linking the parameters of SAXS with the characteristics of certain heterogeneities. Such a parameter in Ref. [64] was external hydrostatic pressure, which can effectively reduce the porosity of a wide range of materials [65-67]. As a rule, application of external hydrostatic pressure leads to a decrease in the average size of pores at their unchanged total concentration. The decrease in the SAXS intensity after applying hydrostatic pressure to AMAs is associated only with the reduced size of those zones, which cause SAXS. No change in the concentration and electron density of scattering inhomogeneities is observed. According to Ref. [68], when only the size of inhomogeneities changes, a certain relation between the change in their size (D) and the change in scattering intensity (I) should be fulfilled. In Ref. [69], this relation is also reported. For the $\mathrm{Co_{60}Fe_{10}Si_{15}B_{10}}$ alloy, it was found that exposure at a pressure of 1 GPa for 10 s led to a decrease in D^5 by 1.73 times, and the scattering intensity decreased by 1.8 times. These estimates confirm that the scattering inhomogeneities are voids. Under the assumption that the observed inhomogeneities are micropores, their volume fraction was estimated. The authors of Ref. [64] observed a significant decrease in the size of the scattering centres after 3 µm thick layers were removed from each side of an amorphous ribbon by electrolytic etching. This indicated a heterogeneous distribution of micropores by size: larger micropores (scattering areas) were concentrated in the surface layers of the ribbon, and smaller ones in the middle layers. Based on the results of SAXS studies, it was concluded that ellipsoidal submicroscopic discontinuities with dimensions of 20-100 nm, heterogeneously distributed over the ribbon cross-section, were present in the AMAs.

Besides, as found out, the high-pressure treatment increased the temperature of annealing embrittlement, *i.e.*, the temperature of the ductile-brittle transition, of amorphous Co- or Fe-based alloys. This effect is ob-

Fig. 7. Typical dependence of room temperature ductility parameter e_i on preliminary 1-hour ageing temperature T_X for Fe-B amorphous alloy [74]

served in almost all amorphous metal and metalloid alloys after annealing above the critical temperature [70].

Within this 'force' model, the melt temperature and the effective quenching rate affect the distribution of FVs by size in different ways. The melt temperature is mainly responsible for the total number



of zones with reduced density, which can be 'frozen' during quenching, as well as for the shift in the size distribution towards larger values with increasing melt temperature. The effective quenching rate is responsible for the actual total number of 'frozen' defects, and for the shift in the distribution towards their finer sizes, as the effective melt cooling rate increases.

In Ref. [71], a structural model of 'annealing embrittlement of amorphous alloys' was first formulated, which took into account the fact that the fracture type changed after annealing above a certain critical temperature. This change was associated with the facilitation of brittle crack nucleation on micropores of relaxation origin, which appeared because of the coagulation of zones with excessive FV. Each amorphous alloy with a certain size distribution of the FV regions has a certain critical temperature of the ductile-brittle transition (*T*), which leads to the appearance of a sufficient number of pores of a critical size, that cause microfracture.

One of the features of AMAs is their high ductility under compression and bending [72]. However, ductility abruptly drops after annealing at temperatures, at which no signs of crystallization are yet observed [73]. On the example of amorphous alloys of the Fe-B system (Fig. 7), it was shown that heating in the amorphous state stability region below the temperature T_X caused complete or partial embritlement at room temperature.

As shown in Ref. [74], $T_{\rm X}$ coincides with the temperature interval, within which the most active relaxation processes occur; these processes lead to a noticeable compaction of the amorphous structure.

Two types of models have been proposed to explain the nature of the annealing embrittlement of amorphous alloys:

- 1. the 'segregation' model [75], which explains the embrittlement by the formation of segregations of metal atoms in some zones of the amorphous matrix;
- 2. the 'crystalline' model [76] relates the embrittlement to the formation of a noticeable long-range order or some crystalline phases in the amorphous matrix.

Each of the above models is based on an indirect experimental database, but none of them is consistent with all the experimental results currently available. For example, the segregation model is not able to describe properly the ductile-brittle transition in amorphous metal-metal alloys. The crystalline model does not agree with experimental data, which show that T_X decreases sharply, when small amounts of surfactants are added to the alloy. As a rule, the conclusion about the adequacy of any of these models is 'structureless', *i.e.*, they are not based on a detailed consideration of the variations of structural features of plastic flow and fracture that occur upon the transition through T_X .

Discussing the experimental results, some authors [77, 78] suggested that the ductile-brittle transition is associated with the structural relaxation of the amorphous state. However, no real mechanism based on the physics of plastic deformation and cracking has yet been proposed to explain how structural relaxation would lead to crucial brittleness of amorphous alloys.

Based on general ideas about the nature of the brittle state, two possible processes [73] should be distinguished, which can lead to the loss of macroscopic ductility of AMAs due to thermal effects. These processes are the reduced susceptibility of the material to plastic flow and easier crack formation and growth. However, the susceptibility of AMAs to plastic deformation remains practically unchanged after annealing above $T_{\rm X}$. Therefore, the phenomenon of annealing embrittlement of amorphous alloys is caused not by inhibition of plastic flow, but by facilitating fracture processes.

For determining the nature of the processes that underlie the fracture mechanics of amorphous alloys and play an important role in the annealing embrittlement, a series of works by H. Kimura and T. Masumoto [79, 80] were important. They used the criterion of local fracture under tension, which was able to describe the mechanics of the ductile-brittle transition in amorphous alloys. Using the $Pd_{78}Cu_6Si_{16}$ alloy as an example, they showed that the loss of AMA ductility after annealing could be explained by a decreased stress needed for microfracture, rather than by sliding hindering. Thus, the ductile-brittle transition during annealing can be explained by a decrease in the microfracture stress below the maximum value of the yield strength in the longitudinal direction. Using the fracture criterion proposed by H. Kimura and T. Masumoto, it can be concluded that the annealing embrittlement of AMAs is associated with the facilitation of the fracture process, rather than with the complication of plastic flow. Obviously, the stress needed for fracture at the microscopic level becomes the most important physical parameter characterizing the susceptibility of amorphous alloys to brittle fracture. The stress needed for fracture at the microscopic level is a structurally sensitive characteristic of the material, which tends to decrease sharply under thermal impact that leads to the annealing embrittlement [81].

Besides the above processes, several more structural relaxation processes have been experimentally found out, which lead to a change in the fracture mechanism and, accordingly, to a sharp decrease in the stresses needed for fracture at the microscopic level under certain thermal impacts.

Amorphous alloys produced by the spraying technique have increased porosity and significantly lower T_X values compared to the same alloys produced by melt quenching [82].

The parameters of alloy production by melt quenching have a significant impact on both the ductility in the initial state and the $T_{\rm X}$ value. A thicker ribbon, which corresponds to a lower melt quenching rate, has a lower $T_{\rm X}$ value. As the melt quenching rate increases (and the ribbon thickness decreases), $T_{\rm X}$ rises [83]. In the phenomenon of annealing embrittlement, the excess free volume and its evolution under thermal impacts upon the amorphous structure play a determining role [87].

F. Spaepen and D. Turnbull suggested [85] that in AMAs without a crystal lattice, dilatation (in particular, tension) contributes to the formation of excess free volume at the crack tip. This leads to a slight increase in the volume of the shear transformation zone, which may be related to the free volume relaxation [86]. In the free volume model, the deformation occurs by atomic movement due to FV diffusion. For plastic deformation to occur in a sample under specified conditions (applied stress, temperature, etc.), there should be a sufficient amount of FV capable of migration. Thus, within the framework of this model, the stress concentration at the crack tip acts as a kind of free volume source that plays the role of dislocations in a crystal.

Since free volume is difficult to measure quantitatively, it is usually estimated by measuring the viscosity of the system. Viscosity allows relating the flow rate $\dot{\epsilon}$ to the local stress σ within the framework of Newton's equation: $\epsilon = \sigma/3r. \tag{1}$

Within the framework of Spaepen's model describing deformation due to free volume migration, the viscosity of AMAs below the glass-transition temperature $T_{\scriptscriptstyle g}$ is given as [50]

$$\eta = kT/vb^{3} \{ \exp(-\delta V^{*}/V_{f}) \exp[\Delta G_{m}/(kT)] \}, \qquad (2)$$

where, instead of the probability of finding a vacancy next to an atom, the probability of finding a cavity or free volume of size V^* is used. This probability is expressed as $\exp(-dV^*/V_f)$ [85], where d is the geometric factor of order one.

Wu and Speipen made an important assumption [87] that the temperature of the ductile-brittle transition (not necessarily the annealing embrit-tlement) in the amorphous $\text{Fe}_{79.3}\text{B}_{16.4}\text{Si}_{4.0}\text{C}_{0.3}$ alloy was associated with some critical V_f value and, thus, with a critical value of η . In the absence of

vacancies, the decrease in the free volume in the equilibrium state can be considered as a consequence of thermal expansion: $V_t = a(T - T_0)$.

The concentration of free volume V_f at the test temperature is determined by the following relationship:

$$V_f = \Delta V_{fs} - \Delta V_{fa} - \Delta V_{fa} - a(T - T_0), \tag{3}$$

where $\mathrm{D}V_{fs}$ is the stress-induced change in free volume; $\mathrm{D}V_{fq}$ is the fraction of free volume frozen upon quenching; $\mathrm{D}V_{fs}$ is the change in free volume during annealing.

Thus, both annealing and lowering the test temperature reduce V_f and increase η , increasing the critical stress of the onset of plastic flow.

In Ref. [88], this approach was complemented by the assumption about the development of zones enriched with metalloid. According to the author, the development of such zones should form regions in the amorphous matrix where the amount of free volume is much smaller than the average for the entire alloy; these regions cause embrittlement during annealing. In Ref. [89], on the example of alloys based on the Cu–Zr system, it was also shown that the main reason for the embrittlement of samples was a decrease in the free volume. According to the authors, it is possible to increase the ductility of embrittled samples by annealing above T_g followed by quenching, which leads to the recovery of free volume.

Crack initiation in a region of reduced density (at a micropore in the extreme case) can be easily predicted on the basis of the model developed in Ref. [90]. The authors of Ref. [90] showed that a region with a reduced elastic modulus can produce a brittle crack when a shear band interacts with a boundary, which separates regions with different moduli. According to this work, when the difference in moduli in neighbouring regions becomes four times, the initiation of a brittle crack becomes spontaneous under external load. Since the free volume region can evolve into a submicroscopic pore at the stage of free volume annihilation, there comes a critical moment when the discontinuity can initiate a crack. The situation can be aggravated by the fact that impurities can segregate at the interface between regions with different densities (and hence different elastic moduli), which reduces the surface energy.

The possibility of diffusion processes under stresses that lead to the disappearance of micropores directly follows from theoretical studies [91]: coarser micropores should disappear at a higher rate than finer micropores because of their filling due to self-diffusion. Besides, it was concluded in Ref. [92] that the free volume is not capable of instant redistribution and requires some time to achieve a new equilibrium distribution, which would lead to the equalization of microstresses over the volume of the amorphous matrix.

5. Thermal Stability and Crystallization of Amorphous Alloys

The study of thermal stability (TS) of AMAs under the impact of external factors and crystallization is of considerable scientific interest. In AMAs, the consistent patterns of crystal nucleation and growth under conditions of extremely non-equilibrium crystallization can be more clearly established as compared to melts. Understanding these processes is also important for the application aspect, since resistance to the onset of crystallization, which leads to a sharp irreversible change in properties, mainly determines the thermal stability and, accordingly, the limits of AMAs' applicability.

According to the modern classification, certain types of crystallization reactions can take place, depending on the chemical composition of an amorphous alloy:

- polymorphic crystallization: an amorphous alloy transforms into a supersaturated solid solution, metastable or stable crystalline phase without changing its composition [93, 94];
- eutectic crystallization: two crystalline phases form simultaneously
 [95];
- primary crystallization: one stable or metastable phase forms at the first stage [96].

The type of reaction that takes place in a particular case is determined by both the thermodynamic driving force and the activation barrier, and hence their kinetics. Since long-range diffusion is involved in the latter type of abovementioned reactions, the rate of crystallite growth decreases over time. As shown in [97], the radius of primary crystals a-Fe in the ${\rm Fe_{86}B_{14}}$ alloy depended parabolically on the annealing time ($r \propto \sqrt{Dt}$, where D is the diffusion coefficient), *i.e.*, growth in this case is controlled by bulk diffusion.

As mentioned above, structural relaxation processes become noticeable when an AMA is heated and the mobility of atoms increases, which leads to a decrease in free energy.

Upon further heating and the transition to more realistic conditions of long-range diffusion of atoms, crystallization processes develop nucleation and growth of crystallites of one or several phases, which leads to sharp changes in all structural parameters and properties of an AMA [98].

The temperature of crystallization onset (T_x) is not a thermodynamic constant for an amorphous alloy [99–101]. This temperature depends primarily on the heating rate, as well as on a number of other factors, such as the quenching method and conditions, thermal history of the amorphous alloy, etc., which determine the structural state of quenched AMAs [102]. On the example of an alloy of the Fe-B–Si–P–Cu system, the authors of Ref. [101] showed that an increase in the heating rate from 5 to 40 °C/min led to a T_x rise by 35 °C. Therefore, it is hardly correct to use

this parameter directly as a measure of the thermal stability of AMAs. Another physical parameter is often considered in this relation—the glass transition temperature (T_a) . Although this temperature is lower than T_{x} , it also depends on the heating rate and cannot always be experimentally determined [19]. Values related to T_{σ} are also used, for example, the criterion of relative stability $DT_k = T_X - T_g$, which characterizes the stability of amorphous phases with the same alloy viscosities [103], or the reduced glass transition temperature $T_{rg} = T_g/T_m$ [104] (for most amorphous alloys, this ratio is within 0.5-0.6 [98]). When AMAs are considered as superviscous frozen melts, it seems more correct to evaluate their thermal stability by the reduced temperature of the crystallization onset $T_{\scriptscriptstyle X}/T_{\scriptscriptstyle m}$. Such an estimate allows comparing the thermal stability of various alloys, which is understood as the probability of preserving the amorphous state at the same supercooling below the liquidus temperature, and is quite convenient in practice. In this case, the T_x values can be easily determined during continuous heating of an amorphous alloy at a constant rate $(V_h = dT/dt = \text{const})$.

To explain the dependence of the thermal stability of amorphous alloys on their composition, as well as to predict this dependence, empirical criteria based mainly on thermodynamic, crystallographic, or electronic factors were proposed [105].

For metal-metalloid systems, it was emphasized that TS is maximal at compositions close to the eutectic concentrations [106]. The strong interaction of the metal and metalloid atoms (as well as the base and alloying metals in transition metal-based AMAs) manifests itself in a large negative mixing enthalpy and contributes to an increase in the reduced temperature of the glass transition T_{rg} [101]. Significantly smaller metal atoms contribute to the stabilization of the structure of the dense random packing of AMAs by occupying interstitial sites [107]. For example, in amorphous alloys of the (Fe, Ni)-M-Si-B system, the temperature of the onset of crystallization increases if the atomic radius of the M element is larger than that of the base metal, and decreases, if it is smaller [108]. An increase in T_x in similar alloys was observed [109] as the negative difference between the charges of the atoms of alloying and base metals increased. Considering an amorphous alloy as a solid with almost free electrons, S.R. Nagel and Y. Tauk [110] showed that the most stable state corresponds to the minimum density of states at the Fermi level. As a consequence of this assumption, the temperature coefficient of electrical resistance of amorphous alloys of compositions that meet this criterion is negative. The analysis of literature data [14] shows that the above criteria adequately describe the experimentally observed patterns, at least for alloys that are close in chemical nature.

The formation of certain crystalline phases during the crystallization of AMAs is determined not only by their thermodynamic parameters, but also by the activation energy of the corresponding processes. Since this energy is usually lower in the case of the formation of metastable phases than stable phases (those indicated in equilibrium diagrams), the crystallization in many amorphous alloys goes through the stage of formation of metastable phases, which then transform into stable phases [14].

In Ref. [14], on the example of alloys of the (Fe, Ni, Co)-B system, it was shown that up to a certain annealing temperature the number of nuclei per unit volume did not depend on the temperature and exposure time. This indicated that the nuclei were already present in the quenched alloy. Since there are ordered zones (pre-nuclei) in the quenched melt with a temperature-dependent size distribution, the coarser ones and then the finer ones become stable during URC through the T_m - T_g interval, as their sizes become larger than the critical one with DT increasing. Thus, the quenched alloy can already contain so-called 'frozen' centres, or quenched nuclei, which can grow when heated to relatively low temperatures, when thermally activated formation of new nuclei is not yet possible for kinetic reasons. This was also shown in Ref. [111], where the dependence of the volume concentration of nuclei on the quenching rate was determined. According to experimental estimates, the density of nuclei can reach $\approx 10^{21}$ m⁻³, depending on the alloy composition and quenching rate [98]. Based on the fact that such a high density of heterogeneous nucleation sites is physically unlikely, it is believed that such values of density of nuclei may indicate homogeneous crystallization.

Heat treatment before quenching determines the initial melt structure. The quenching rate determines the degree of nonequilibrium of the resulting structure of the quenched alloy and the possibility of crystallization during quenching. As a result, the amorphous alloy can contain different concentrations of the described 'frozen' centres, as well as free volume and so on.

Features of the heating modes of amorphous alloys for studying their crystallization can also significantly affect the results obtained. In particular, the structural relaxation processes described above can occur during the heating of the sample to the annealing temperature, especially at high temperatures; these processes significantly change such material characteristics as atomic mobility, free energy, etc. [14].

The kinetics of isothermal crystallization of amorphous alloys is described using the Johnson-Mehl-Avrami expression in the general form [112]:

$$X(t) = 1 - \exp[-K(t - t_0)n], \tag{4}$$

where n is the Avrami exponent, which is determined by the mechanisms of nucleation and morphology of crystal growth (according to theoretical concepts, it is in the range 1.5–4); t_0 is the incubation time; K is the reaction rate constant for which the Arrhenius law is assumed valid [112]:

$$K = K_0 \exp(-E_0/RT). \tag{5}$$

In the last expression, E_a is the effective activation energy of the entire crystallization process. Double logarithmization of Eq. (4) allows transforming it [112] into

$$\ln[-\ln(1-X)] = n\ln t + \text{const},\tag{6}$$

so, it can be seen that linearization of the experimental kinetic curve in the co-ordinates $\ln[-\ln(1-X)]$ and $\ln t$ makes it possible to determine n for each section of this dependence. Although knowing only the value of n, especially taking into account the above, does not allow unambiguous determination of the crystallization mechanism.

The assumption of the validity of the Arrhenius temperature dependence for describing the processes of nucleation and growth during the crystallization of amorphous alloys is also the basis for the analysis of this transformation under non-isothermal conditions, which is generally accepted to date [113].

The increase in the temperature of the onset of crystallization of amorphous alloys with increasing heating rate allows determining the value of the total activation energy of the crystallization following the Kissinger's equation [113]:

$$\ln(V_H/T_r^2)] = -E/RT_r + C, (7)$$

where T_x is the temperature of some characteristic moment of the process (most often, either the temperature of the crystallization start T_x , or the temperature of the maximum rate of transformation (for thermoanalytical methods)).

The validity of using Eq. (7) to describe the non-isothermal crystallization of amorphous alloys has been analysed and confirmed by many researchers with some assumptions [114, 115].

6. Conclusions

It is determined that the characteristic structural feature of all amorphous alloys is the presence of free volume (FV) in them, since the density of the alloy in the amorphous state is always lower than in the crystalline state. Free volumes (FVs) are the low-density zones characterized by a certain size distribution (from fractions of an atomic diameter to hundreds of nanometres) which depends on the conditions of production, composition, heat treatment and a number of other factors.

Alloys in the amorphous state, due to the absence of translational symmetry (long-range order) and, accordingly, stacking faults, have better properties than in the crystalline state: high strength and hardness combined with high ductility; high corrosion and abrasive wear resistance; high specific electrical resistance at low, and even sometimes negative (in °C), temperatures and thermal coefficient; high magnetic permeability; low coercive force.

Acknowledgements. This work was carried out as part of the research work 'Structural and phase states and physical and mechanical properties of precision Co-Ni-Cr and Ni-TiC superalloys and protective coatings based on them for the machine-building and energy industries' for 2025–2029 (state reg. No. 0124U002939).

REFERENCES

- A. Brenner, D.E. Couch, and E.K. Williams, Electrodeposition of Phosphorous with Nickel or Cobalt, J. Res. Natl. Bur. Stand., 44: 109-122 (1950); https://doi.org/10.6028/ires.044.009
- W. Klement, R.H. Willens, and P. Duwez, Non-Crystalline Structure in Solidified Gold-Silicon Alloys, *Nature*, 187: 869–870 (1960); https://doi.org/10.1038/187869b0
- C. Fu, L. Sun, and Z. Cheng, Molecular Dynamics Simulation of Glass Forming Ability of Al₃₀Co₁₀ Amorphous Alloy, J. Appl. Sci., 5: 552-558 (2015); https://doi.org/10.4236/ojapps.2015.59053
- 4. N. Abdelhakim, R. Shalaby, and M. Kamal, A Study of Structure, Thermal and Mechanical Properties of Free Machining Al–Zn–Sn–Bi Alloys Rapidly Solidified from Molten State, *World J. Eng. Technol.*, 6: 637–650 (2018); https://doi.org/10.4236/wjet.2018.63040
- Q. Yu and G. Wu, A Binder-Free Amorphous Manganese Dioxide for Aqueous Zinc-Ion Battery, J. Mat. Sci. Chem. Eng. A, 10: 13-18 (2022); https://doi.org/10.4236/msce.2022.106002
- S.A. Kube, P. Bordeenithikasem, P. Ziemke, J. Lamb, J. Rossin, C. Torbet, M.R. Begley, R. P. Dillon, and T.M. Pollock, Non-Destructive Evaluation of Bulk Metallic Glass Components Using Resonance Ultrasound Spectroscopy, *Applied Mater. Today*, 42: 102529 (2025);
 - https://doi.org/10.1016/j.apmt.2024.102529
- Q. Yang, B. Wang, Z. Zhao, H. Zhao, Q. Bu, J. Li, P. Yu, and H. Yu, Vapor-Deposited High-Entropy Metallic Glasses, *J Phys. Chem. B*, 129: 456-464 (2025); https://doi.org/10.1016/10.1021/acs.jpcb.4c04677
- 8. C. Zhang, D. Ouyang, S. Pauly, and L. Liu, 3D Printing of Bulk Metallic Glasses, *Mater. Sci. Eng. R*, **145**: 100625 (2021); https://doi.org/10.1016/j.mser.2021.100625
- 9. W. Ming, X. Guo, Y. Xu, G. Zhang, Z. Jiang, Y. Li, and X. Li, Progress in Non-Traditional Machining of Amorphous Alloys, *Ceram. Int.*, **49**: 1585–1604 (2023); https://doi.org/10.1016/j.ceramint.2022.10.349
- S. Sohrabi, J. Fu, L. Li, Y. Zhang, X. Li, F. Sun., J. Ma, and W.H. Wang, Manufacturing of Metallic Glass Components: Processes, Structures and Properties, Prog. Mater Sci., 144: 101283 (2024); https://doi.org/10.1016/j.pmatsci.2024.101283
- 11. X. Wang, S. Yu, N. Chen, Y. Chao, X. Jiang, and D. Yu, Optimizing Ni-Zr-Ti Metallic Glasses: Cluster Design and Molecular Dynamics Evaluation of Glass Forming Ability, *J. Alloys Compd.*, **1009**: 177007 (2024); https://doi.org/10.1016/j.jallcom.2024.177007
- W.L. Johnson, Bulk Amorphous Metal-An Emerging Engineering Material, JOM, 54, No. 3: 40-43 (2002); https://doi.org/10.1016/10.1007/BF02822619

- 13. M. Frey, R. Busch, W. Possart, and I. Gallino, On the Thermodynamics, Kinetics, and sub-Tg Relaxations of Mg-Based Bulk Metallic Glasses, *Acta Mater.*, **155**: 117–127 (2018);
 - https://doi.org/10.1016/j.actamat.2018.05.063
- 14. V.V. Kyrylchuk, Effect of Transition Metal Alloying on Thermal Stability, Structural Relaxation, Crystallization and Magnetic Properties of Amorphous CoSiB Alloys (Abstract of Diss. Candidate of Physical and Mathematical Sciences) (Kyiv: G.V. Kurdyumov Institute for Metal Physics, N.A.S.U.: 2021) (in Ukrainian).
- 15. V.I. Tkatch, A.I. Limanovskii, S.N. Denisenko, and S.G. Rassolov, The Effect of the Melt-Spinning Processing Parameters on the Rate of Cooling, *Mater. Sci. Eng.* A, 323: 91–96 (2002);
 - https://doi.org/10.1016/S0921-5093(01)01346-6
- R.C. Ruhl, Cooling Rates in Splat Cooling, Mater. Sci. Eng. A, 1: 313–320 (1967); https://doi.org/10.1016/0025-5416(67)90013-4
- 17. Y. Sun, A. Concustell, and A.L. Greer, Thermomechanical Processing of Metallic Glasses: Extending the Range of the Glassy State, *Nat. Rev. Mater.*, 1: 16039 (2016); https://doi.org/10.1038/natrevmats.2016.39
- X. Yuan, Y. Zhang, X. Qu, H. Yin, S. Li, Z. Yan, Z. Tan, S. Hu, Y. Gao, and P. Guo, A Review of the Preparation and Prospects of Amorphous Alloys by Mechanical Alloying, J. Mater. Res. Technol., 33: 3117-3143 (2024); https://doi.org/10.1016/j.jmrt.2024.10.026
- 19. Si. Yamaura, W. Zhang, and A. Inoue, Introduction to Amorphous Alloys and Metallic Glasses (Eds. Y. Setsuhara, T. Kamiya, T., and S. Yamaura) *Novel Structured Metallic and Inorganic Materials* (Singapore: Springer: 2019), p. 3–22; https://doi.org/10.1007/978-981-13-7611-5
- 20. M.O. Vasylyev, V.K. Nosenko, I.V. Zagorulko, and S.M. Voloshko, Nanocrystallization of Amorphous Fe-Based Alloys under Severe Plastic Deformation, *Prog. Phys. Met.*, 21, No. 3: 319–344 (2020); https://doi.org/10.15407/ufm.21.03.319
- 21. F. Gaskell, Models of the Structure of Amorphous Metals, Metallic Glasses. Vol. 2 (Eds. G. Beka and G. Guntherodt) (Moskva: Mir: 1986) (in Russian).
- 22. O.I. Mitsek and V.M. Pushkar, Cluster Model of Liquid or Amorphous Metal. Quantum-Statistical Theory. Amorphous Metal, Metallofiz. Noveishie Tekhnol., 36, No. 1: 103-125 (2014) (in Russian); https://doi.org/10.15407/mfint.36.01.0103
- 23. R. Su, J. Yu, P. Guan, and W. Wang, Efficient and Accurate Simulation of Vitrification in Multicomponent Metallic Liquids with Neural Network Potentials, *Sci. China Mater.*, 67, No. 10: 3298-3308 (2024); https://doi.org/10.1007/s40843-024-2953-9
- 24. V. Ankudinov, K. Shklyaev, and M. Vasin, Mesoscopic Glass Transition Model: Influence of the Cooling Rate on the Structure Refinement, *AIMS Mathematics*, 9, No. 8: 22174–22196 (2024); https://doi.org/10.3934/math.20241078
- 25. J.D. Bernal, Geometry of the Structure of Monoatomic Liquids, *Nature*, **185**: 68–70 (1960);
 - https://doi.org/10.1038/185068a0
- 26. Z.H. Stachurski, On Structure and Properties of Amorphous Materials, *Materials*,
 4: 1564–1598 (2011);
 - https://doi.org/10.3390/ma4091564
- 27. J.A. Prins, *Physics of Non-Crystalline Solids* (North-Holland Publishing Company: 1965).

- 28. C.L. Briant and J.J. Burton Icosahedral Microclusters a Possible Structural unit in Amorphous Metals, *Phys. Stat. Sol. B*, **85**: 393–402 (1978); https://doi.org/10.1002/pssb.2220850144
- 29. M. Kramer and M. Li, Changes in Short- and Medium-Range order in Metallic Liquids during Undercooling, *MRS Bulletin*, **45**: 943-950 (2020); https://doi.org/10.1557/mrs.2020.272
- 30. A.S. Bakai, Polycluster Amorphous Solids (Kharkiv: Syntex: 2013) (in Russian).
- 31. W.L. Johnson and A.R. Williams, Structure and Properties of Transition Metal-Metalloid Glasses Based on Refractory Metals, *Phys. Rev.*, **20**, No. 4: 1640–1655 (1979); https://doi.org/10.1103/PhysRevB.20.1640
- 32. A.V. Romanova and I.G. Ilyinsky, Structure of Amorphous Metallic Alloys, *Amorphous Metallic Alloys* (Kyiv: Naukova Dumka: 1987) (in Russian).
- 33. A.V. Romanova, V.V. Nemoshkalenko, G.M. Zelinskaya, A.G. Ilyinsky, V.V. Bukhalenko, and A.I. Senkevich, Study of the Structure of Iron-Boron Metallic Glasses, *Metallofizika*, 5, No. 4: 49-56 (1983) (in Russian).
- 34. Y. Hirotsu, R. Akada, High Resolution Electron Microscopy Observation of Microcrystalline Domains in Amorphous Fe₈₄B₁₆ Alloy, Jap. J. Appl. Phys., 23, No 7: 479–481 (1984); https://doi.org/10.1143/JJAP.23.L479
- 35. K. Kriљtiakovó, J. Kriљtiak, P. Pacher, and V. Simkin, Neutron Diffraction Study of Fe₈₃B₁₇ Metallic Glass, *Czech J. Phys.*, 41: 1153–1159 (1991); https://doi.org/10.1007/BF01598991
- 36. I.V. Zolotukhin, Amorphous Metallic Materials, Soros Educational J., 4: 73-78 (1997) (in Russian).
- 37. A. Jabed, M.N. Bhuiyan, W. Haider, and I. Shabib, Distinctive Features and Fabrication Routes of Metallic-Glass Systems Designed for Different Engineering Applications: A Review, *Coatings*, 13, No. 10: 1689 (2023); https://doi.org/10.3390/coatings13101689
- D.A. Kalashnik, V.A. Shapovalov, I.V. Sheiko, Yu.A. Nikitenko, and V.V. Yakusha, Analysis of Technological Peculiarities of Producing Rapidhardening Aloys (Review), *Electrometallurgy Today*, 3: 27–34 (2015) (in Russian); https://doi.org/10.15407/sem2015.03.05
- 39. Y. Wu, Q. Luo, J. Jiao, X. Wei, and J. Shen, Investigating the Wear Behavior of Fe-Based Amorphous Coatings under Nanoscratch Tests, *Metals*, 7: 118 (2017); https://doi.org/10.3390/met7040118
- 40. G. Kisfaludi, Z. Schay, and L. Guczi, Surface Structure and Satalytic Activity of Rapidly Quenched Amorphous Iron Based Alloys: II. Effect of Hydrochloric Acid Treatment, Appl. Surface Sci., 29: 367-379 (1987); https://doi.org/10.1016/0169-4332(87)90040-7
- 41. C. Gao, S. Tang, S. Zhao, Z. Zhao, H. Pan, and C. Shuai, Amorphous/Crystalline Zn₆₀Zr₄₀ Alloys Lattice Structures with Improved Mechanical Properties Fabricated by Mechanical Alloying and Selective Laser Melting, *Virtual Phys. Protot.*, 18, No. 1: e2220549 (2023); https://doi.org/10.1080/17452759.2023.2220549
- 42. P.N. Vyugov and A.E. Dmitrenko, Metallic Glasses, *Problems of Atomic Science and Technology*, 6, No. 14: 185–191 (2004) (in Russian).
- 43. I.V. Zolotukhin and Yu.V. Barmin, Stability and Relaxation Processes in Metallic Glasses (Moskva: Metallurgiya: 1991) (in Russian).
- M.R.J. Gibbs, J.E. Evetts, and J.A. Leake, Activation Energy Spectra and Relaxation in Amorphous Materials, J. Mater. Sci., 18: 278–288 (1983); https://doi.org/10.1007/BF00543836

- 45. P. Kruger, L. Kempen, and H. Neuhauser, Determination of the Effective Attempt Frequency of Irreversible Structural Relaxation Processes in Amorphous Alloys by Anisothermal Measurements, *Phys. Stat. Sol. A*, **131**: 391–402 (1992); https://doi.org/10.1002/pssa.2211310213
- P. Roura and J. Farjas, Structural Relaxation Kinetics for First- and Second-Order Processes: Application to Pure Amorphous Silicon, *Acta Mater.*, 57, No. 7: 2098–2107 (2009);
 - https://doi.org/10.1016/j.actamat.2009.01.011
- 47. G.W. Koebrugge, J. Van der Stel, J. Sietsma, and A. Van den Beukel, Effect of the Free Volume on the Kinetics of Chemical Short-Range Ordering in Amorphous Fe₄₀Ni₄₀B₂₀, J. Non-Cryst. Sol., 117–118, No. 2: 601–604 (1990); https://doi.org/10.1016/0022-3093(90)90604-K
- 48. A. Van den Beukel and J. Sietsma, Diffusivity and Viscosity During Structural Relaxation in Metallic Glasses, *Mater. Sci. Eng. A*, 179–180: 86–90 (1994); https://doi.org/10.1016/0921-5093(94)90170-8
- 49. T. Egami and V. Vhtek, Local Structural Fluctuations and Defects in Metallic Glasses, *J. Non-Cryst. Sol.*, **61–62**, No. 4: 499–510 (1984); https://doi.org/10.1016/0022-3093(84)90596-9
- 50. F. Spaepen, A Microscopic Mechanism for Steady State Inhomoheneous Flow in Metallic Glasses, *Acta Metall.*, 25, No. 3: 407–415 (1977); https://doi.org/10.1016/0001-6160(77)90232-2
- 51. A.I. Taub and F. Spaepen, The Kinetics of Structural Relaxation of a Metallic Glass, *Acta Metall.*, 28, No. 10: 1781-1788 (1980); https://doi.org/10.1016/0001-6160(80)90031-0
- 52. F. Spaepen and A.I. Taub, Plastic Flow and Destruction, *Amorphous Metallic Alloys* (Moskva: Metallurgiya: 1987) (Russian translation).
- A.T. Kosilov, V.A. Khonic, and V.A. Mikhailov, The Kinetics of Stress-Oriented Structural Relaxation in Metallic Glasses, J. Non-Cryst. Sol., 192–193: 420–423 (1995); https://doi.org/10.1016/0022-3093(95)00385-1
- 54. H. Zhou, V. Khonik, and G. Wilde, On the Shear Modulus and Thermal Effects during Structural Relaxation of a Model Metallic Glass: Correlation and Thermal Decoupling, *J. Mater. Sci. Technol.*, **103**: 144–151 (2022); https://doi.org/10.1016/j.jmst.2021.05.081
- 55. A. Van den Beukel, E. Huizer, A.L. Mulder, and S.A. Van der Zwaag, Change of Viscosity during Structural Relaxation Fe₄₀Ni₄₀B₂₀, Acta Metall., 34, No. 3: 483– 492 (1986);
- 56. A. Van den Beukel and J. Sielsma, On the Nature of the Glass Transition in Metallic Glasses, *Phil. Mag. B*, **61**, No. 4: 539–547 (1990); https://doi.org/10.1080/13642819008219292
- 57. G.W. Koebrugge, J. Sietsma, and A. Van den Beukel, Structural Relaxation and Equilibrium Free Volume in Amorphous Pd₄₀Ni₄₀B₂₀, J. Non-Cryst. Sol., 117–118, No. 2: 609–612 (1990);
 - https://doi.org/10.1016/0022-3093(90)90606-M

https://doi.org/10.1016/0001-6160(86)90084-2

- 58. G. Knuyt, H. Stulens, W. De Ceuninck, and L.M. Stals, Derivation of an Activation Energy Spectrum for Defect Processes From Isothermal Measurements, Using a Minimization Principle and Fourier Analysis, *Modeling Simul. Mater. Sci. Eng.*, 1: 437–448 (1993);
 - https://doi.org/10.1088/0965-0393/1/4/007
- 59. A. Kasardova, V. Ocelik, K. Csach, and J. Miskuf, Activation Energy Spectra for Stress-Induced Ordering in Amorphous Materials Calculated Using Fourier

- Techniques, *Phil. Mag. Lett.*, **71**, No. 5: 257–261 (1995); https://doi.org/10.1080/09500839508240518
- 60. A.M. Glezer and B.V. Molotilov, Structure and Mechanical Properties of Amorphous Alloys (Moskva: Metallurgiya: 1992) (in Russian).
- 61. I.I. Shtablavyi, Correlations of Free Volume and Short-Range Order Structure in Metallic Melts with Different Degrees of Microheterogeneity of Atomic Distribution (Abstract of Diss. Doctor of Physical and Mathematical Sciences) (Lviv: Ivan Franko National University of Lviv, Ministry of Education and Science of Ukraine: 2020) (in Ukrainian).
- 62. A.M. Glezer and V.I. Betechtin, Free Volume and Mechanisms of Destruction of Amorphous Alloys, *Solid State Physics*, 38, No. 6: 1784-1790 (1996) (in Russian).
- 63. G.E. Abrosimova and A.S. Aronin, Free Volume in Amorphous Alloys and Its Change under External Influences, J. Surf. Invest., 17: 934-941 (2023). https://doi.org/10.1134/S1027451023040201
- 64. V.I. Betechtin A.M. Glezer, A.G. Kadomtsev, and A.Yu. Kipyatkova, Excess Free Volume and Mechanical Properties of Amorphous Alloys, *Solid State Physics*, 40, No. 1: 85–89 (1998) (in Russian).
- 65. V. Sklenicka, V.I. Betekhtin, K. Kucharova, A.G. Kadomtsev, and A.I. Petrov, Shrinkage of Creep Cavities in Copper by Application of High Hydrostatic Pressure at Ambient Temperature, *Scripta Metall. Mater.*, 25: 2159–2164 (1991); https://doi.org/10.1016/0956-716X(91)90292-9
- 66. J. Dvorak, V. Sklenicka, V.I. Betekhtin, A.G. Kadomtsev, P. Kral, M. Kvapilova, and M. Svoboda, The Effect of High Hydrostatic Pressure on Creep Behaviour of Pure Al and a Cu-0.2 wt% Zr Alloy Processed by Equal-Channel Angular Pressing, *Mater. Sci. Eng. A*, 584: 103-113 (2013); https://doi.org/10.1016/j.msea.2013.07.018
- 67. V. Sklenicka, J. Dvorak, P. Kral, V.I. Betekhtin, A.G. Kadomtsev, M.V. Narykova, S.V. Dobatkin, K. Kucharova, and M. Kvapilova, Influence of a Prior Pressurization Treatment on Creep Behaviour of an Ultrafine-Grained Zr-2.5% Nb Alloy, *Mater. Sci. Eng. A*, 820: 141570 (2021); https://doi.org/10.1016/j.msea.2021.141570
- 68. A. Guinier and G. Fournet, Small-Angle Scattering of X-Rays (New York: John Wiley and Sons: 1955).
- 69. V.I. Betekhtin, A.G. Kadomtsev, V.A. Konkova, and A.I. Petrov, *Accumulation and Healing of Cracks in Deformed Aluminum* (Preprint of the Phys.-Tech. Inst. No. 1076, 18 1986) (in Russian).
- H.H. Liebermann and C.D. Graham, Production of Amorphous Alloy Ribbons and Effects of Apparatus Parameters on Ribbon Dimensions, *IEEE Trans. Magn.*, 12, No. 6: 921–923 (1976); https://doi.org/10.1109/TMAG.1976.1059201
- 71. A.M. Glezer, B.V. Molotilov, and O.L. Utevskaya, Parameters of Structural Relaxation and Mechanical Properties of Amorphous Alloys, *Fiz. Met. Metalloved.*, 57, No. 6: 1198–1210 (1984) (in Russian).
- 72. X. Liu, J. Kong, X. Song, S. Feng, Z. Zhang, Y. Yang, and T. Wang, Free Volume Evolution Dominated by Glass Forming Ability Determining Mechanical Performance in Zr_xTi_{65-x}Be_{27.5}Cu_{7.5} Metallic Glasses, *Mater. Sci. Eng. A*, 804: 140764 (2021); https://doi.org/10.1016/j.msea.2021.140764
- V.A. Fedorov, A.V. Yakovlev, and A.N. Kapustin, Effect of Annealing on the Kinetics of Embrittlement of Amorphous Alloys, Met. Sci. Heat. Treat., 50: 397– 399 (2008);
 - https://doi.org/10.1007/s11041-008-9058-8

- 74. A.M. Glezer, The Problem of Ductile-Brittle Transition of Amorphous Alloys, *J. de Phys. IV: JP*, 8, No. 8: 175–180 (1998); https://doi.org/10.1051/jp4:1998822
- 75. C.A. Pampillo and D.E. Polk, Annealing Embrittlement in an Iron-Nickel-Based Metallic Glasses, *J. Mater. Sci. Eng. A*, 33, No. 2: 275-280 (1978); https://doi.org/10.1016/0025-5416(78)90181-7
- 76. F.E. Fujita, On the Intermediate Range Ordering in Amorphous Structure, *Proc. Fourth Int. Conf. RAM (Sendai, Japan)*, vol. 1, p. 301-304 (1981).
- 77. T. Egami, Strucrural Relaxation and Magnetism in Amorphous Alloys, *J. Magn. Magn. Mater.*, 31–34, No. 3: 1571–1574 (1983); https://doi.org/10.1016/0304-8853(83)91019-3
- 78. J. Gondro, Influence of the Microstructure on the Magnetic Properties of Fe₈₆Zr₇Nb₁Cu₁B₅ Alloy in the States Following Solidification and Following Short-Duration Annealing Below the Crystallization Temperature, *J. Magn. Magn. Mater.*, 432: 501-506 (2017); https://doi.org/10.1016/j.jmmm.2017.02.035
- 79. H. Kimura and T. Masumoto, Deformation and Fracture of an Amorphous Pd-Cu-Si Alloy in V-notch Bending Test. I. Model Mechanics of Inhomogeneous Plastic Flow in on-strain Hardening Solids, *Acta Metall.*, 28, No. 7: 1663–1675 (1980); https://doi.org/10.1016/0001-6160(80)90020-6
- 80. H. Kimura and T. Masumoto, Deformation and Fracture of an Amorphous Pd-Cu-Si Alloy in V-notch Bending Test. II. Ductile-Brittle Transition, *Acta Metall.*, 28, No. 7: 1677-1693 (1980); https://doi.org/10.1016/0001-6160(80)90021-8
- A.M. Glezer, A.I. Potekaev, and A.O. Cheretaeva, Thermal and Time Stability of Amorphous Alloys (Boca Raton: CRC Press: 2017); https://doi.org/10.1201/9781315158112
- 82. T. Masumoto, Mechanical Characteristics of Amorphous Metals, Sci. Rep. RITU, 26: 246-262 (1977); https://doi.org/10.50974/00042941
- 83. O.L. Kravets, A.B. Lysenko, and T.V. Kalinina, Features of the Formation of the Structure of the Fe₈₀B₂₀ Alloy, Nanosistemi, Nanomateriali, Nanotehnologii, 8, No. 3: 535–545 (2010) (in Russian); https://www.imp.kiev.ua/nanosys/en/articles/2010/3/nano_vol8_iss3_p0535p0545_2010_abstract.html
- 84. C. Minnert, M. Kuhnt, S. Bruns, A. Marshal, K.G. Pradeep, M. Marsilius, E. Bruder, and K. Durst, Study on the Embrittlement of Flash Annealed Fe_{85.2}B_{9.5}P₄Cu_{0.8}Si_{0.5} Metallic Glass Ribbons, *Mater. Des.*, **156**: 252–261 (2018); https://doi.org/10.1016/j.matdes.2018.06.055
- 85. F. Spaepen and D. Turnbull, A Mechanism for the Flow and Fracture of Metallic Glasses, *Scr. Metall.*, 8, No. 2: 563–568 (1974); https://doi.org/10.1016/0036-9748(74)90070-2
- 86. R.T. Qu, M. Stoica, J. Eckert, and Z.F. Zhang, Tensile Fracture Morphologies of Bulk Metallic Glass, J. Appl. Phys., 108: 063509 (2010); https://doi.org/10.1063/1.3487968
- 87. T.V. Wu and F. Spaepen, Small Angle X-ray Scattering from an Embrittling Metallic Glass, *Acta Metall.*, 33, No. 11: 2185–2187 (1985); https://doi.org/10.1016/0001-6160(85)90179-8
- 88. A.R. Yavari, Formation of Boron-rich Zones and Embrittlement of Fe-B-Type Metallic Glasses, J. Mater. Res., 1, No 6: 746-751 (1986); https://doi.org/10.1017/S0884291400120059

- 89. F. Jiang, Y. Zhao, L. Zhang, S. Pan, Y. Zhou, L. He, and J. Sun, Dependence of Ductility on Free Volume in a Cu–Zr-Based Metallic Glass, *Adv. Eng. Mater.*, 11, No. 3: 177–181 (2009); https://doi.org/10.1002/adem.200800262
- 90. V.A. Soloviev and V.G. Gryaznov, Criterion of Dislocation Nucleation of Cracks Near Interphase Boundaries, *Doklady AN SSSR*, 301, No. 3: 614–617 (1988) (in Russian).
- 91. L.N. Larikov, *Healing of Defects in Metals* (Kiev: Naukova Dumka: 1980) (in Russian).
- 92. A.I. Taub, Measurement of Microscopic Volume Strain Element in Amorphous Alloys, *Scr. Metall.*, 17, No. 7: 873-878 (1983); https://doi.org/10.1016/0036-9748(83)90252-1
- 93. U. Kester and U. Herold, Crystallization of Metallic Glasses (Metallic Glasses: Ionic Structure, Electron Transfer and Crystallization) (Moskva: Metallurgiya: 1983) (Russian translation).
- 94. G. Abrosimova and A. Aronin, Amorphous and Nanocrystalline Metallic Alloys, Progress in Metallic Alloys (2016); https://doi.org/10.1134/10.5772/64499
- 95. V.I. Tkatch, K.A. Svyrydova, S.V. Vasiliev, and O.V. Kovalenko, Relation Between the Structural Parameters of Metallic Glasses at the Onset Crystallization Temperatures and Threshold Values of the Effective Diffusion Coefficients, *Phys. Metals Metallogr.*, 118: 764-772 (2017); https://doi.org/10.1134/S0031918X17080142
- 96. V.I. Tkatch, V.K. Nosenko, T.N. Moiseeva, S.G. Rassolov, O.V. Kovalenko, M.S. Nizameev, and K.A. Svyrydova, Nanocrystallization and Thermal Stability of the Fe₄₅Ni_{19.4}Co_{8.5}Cr_{5.7}Mo_{1.9}B₁₄Si_{5.5} Amorphous Alloy, J. Non-Cryst. Sol., 430: 108-114 (2015); https://doi.org/10.1016/j.jnoncrysol.2015.09.027
- 97. U. Kester and U. Herold, Effect of Substitution of Metal or Metalloid in Amorphous Iron-Boron Alloys on Their Crystallization, *Fast-Hardened Metals* (Ed. B. Cantor) (Moskva: Metallurgiya: 1987) (Russian translation).
- 98. I.V. Zagorulko, Formation of Metastable Crystalline, Conditionally and Truly Amorphous Structures under Rapid Cooling of the Melts (Diss. Candidate of Physical and Mathematical Sciences) (Dnipro: Oles Honchar Dnipro National University of the Ministry of Education and Science of Ukraine: 2017) (in Ukrainian).
- 99. W.Z. Chen and P.L. Ryder, X-Ray and Differential Scanning Calorimetry Study of the Crystallization of Amorphous Fe_{73.5}Cu₁Nb₃Si_{13.5}B₉ Alloy, *Mater. Sci. Eng. B*, 24: 204-209 (1995); https://doi.org/10.1016/0921-5107(95)01242-7
- 100. K.K. Song, P. Gargarella, S. Pauly, G.Z. Ma, U. Кыhn, and J. Eckert, Correlation Between Glass-forming Ability, Thermal Stability, and Crystallization Kinetics of Cu–Zr–Ag Metallic Glasses, *J Appl. Phys.*, 112, No. 6: 063503 (2012); https://doi.org/10.1063/1.4752263
- 101. M.O. Vasylyev, B.M. Mordyuk, I.V. Zagorulko, S.M. Voloshko, and V.K. Nosenko, Heat Effects in Rapidly-Quenched NANOMET Type Ribbons after Intense Plastic Deformation, *Metallofiz. Noveishie Tekhnol.*, 45, No. 3: 293-310 (2023) (in Ukrainian); https://doi.org/10.15407/mfint.45.03.0293
- 102. J. Zhang, P. Shi, A. Chang, T. Zhao, W. Li, C. Chang, J. Jia, Q. Wang, F. You, D. Feng, X. Wang, Y. Zhao, T. Li, Y. Huang, and S. An, Glass-forming Ability, Thermal Stability, Mechanical and Electrochemical Behavior of Al-Ce-TM

- (TM = Ti, Cr, Mn, Fe, Co, Ni and Cu) Amorphous Alloys, J. Non-Cryst. Solids X, 1:100005 (2019);
- https://doi.org/10.1016/j.nocx.2018.100005
- 103. A. Dunst, D.M. Herlach, and F. Giessen, Formation of Glassy Spheres of Fe-Ni-P-B by Containerless Processing, *Mater. Sci. Eng. A*, 133: 785-789 (1991); https://doi.org/10.1016/0921-5093(91)90186-Q
- 104. A. Takeuchi and A. Inoue, Calculations of Dominant Factors of Glass-Forming Ability for Metallic Glasses from Viscosity, *Mater. Sci. Eng. A*, 375–377: 449–454 (2004); https://doi.org/10.1016/j.msea.2003.10.199
- 105. H.G. Mukhin, Metastable and Nonequilibrium Materials and Their Stability. (Metastable and Nonequilibrium Alloys) (Moskva: Metallurgiya: 1998) (in Russian).
- 106. R. Ray, R. Hasegawa, C.P. Chou, and L.A. Davis, Iron-Boron Glasses: Density, Mechanical and Thermal Behavior, Scr. Metall., 11: 973-978 (1977); https://doi.org/10.1016/0036-9748(77)90249-6
- 107. Y. Cai, B. Lin, Y. Wang, R. Umetsu, D. Liang, S. Qu, Y. Zhang, J. Wang, and J. Shen, Relationship Among Intrinsic Magnetic Parameters and Structure and Crucial Effect of Metastable Fe₃B Phase in Fe-Metalloid Amorphous Alloys, J. Mat. Sci. Technol., 180: 141–149 (2024); https://doi.org/10.1016/j.jmst.2023.07.079
- 108. A. Lovas, L. Granasy, K. Zambo-Balla, and J. Kiraly, Influence of Transition-Metal Additives on the Thermal Stability of Fe₅₀TM₃B₁₇ Quasi-Eutectic Metallic Glasses, Proc. Conf. Metallic Glasses: Science and Technology (Budapest: Hungary), vol. 2, p. 291–297 (1981).
- 109. A. Inoue, K. Kobayashi, J. Kanehira, and T. Masumoto, Mechanical Properties and Thermal Stability of (Fe, Co, Ni)–M–B (M = IV, V and VI-Group Transition Metals) Amorphous Alloys with Low Boron Concentration, Sci. Rep. RITU, 29, No. 2: 331–342 (1981); https://doi.org/10.1016/10.50974/00043247
- 110. S.R. Nagel and Y. Tauk, Influence of the Electronic Structure on the Glass-Forming Ability of Alloys, *Liquid Metals* (Moskva: Metallurgiya: 1980) (in Russian).
- 111. A.L. Greer, Crystallization Kinetics of $Fe_{80}B_{20}$ Glass, *Acta Metall.*, **30**, No. 2: 171–192 (1982); https://doi.org/10.1016/0001-6160(82)90056-6
- 112. J.W. Christian, *The Theory of Transformations in Metals and Alloys* (Moskva: Mir: 1978), Pt. 1 (Russian translation).
- 113. H.E. Kissinger, Reaction Kinetics in Differential Thermal Analysis, *Anal. Chem.*, 29, No. 11: 1702–1706 (1957); http://dx.doi.org/10.1021/ac60131a045
- 114. J.M. Criado and A. Ortega, Non-Isothermal Crystallization Kinetics of Metal Glasses: Simultaneous Determination of Both the Activation Energy and the Exponent *n* of the JMA Kinetic Law, *Acta Metall.*, 35, No. 7: 1715–1721 (1987); https://doi.org/10.1016/0001-6160(87)90117-9
- 115. T. Kemeny and J. Sestak, Comparison of Crystallization Kinetics Determined by Isothermal and Non-Isothermal Methods, *Thermochim. Acta*, 110: 113-129 (1987);
 - https://doi.org/10.1016/0040-6031(87)88217-5

Received 07.02.2025 Final version 01.08.2025 В.А. Дехтяренко^{1,2}, В.К. Носенко¹, В.В. Кирильчук¹, А.В. Носенко¹, О.М. Семирга¹, І.К. Євлаш¹, В.І. Бондарчук¹ Інститут металофізики ім. Г.В. Курдюмова НАН України, бульв. Академіка Вернадського, 36, 03142 Київ, Україна ² Інститут електрозварювання ім. Є.О. Патона НАН України, вул. Казимира Малевича, 11, 03150 Київ, Україна

АМОРФНІ СПЛАВИ ЯК ПЕРСПЕКТИВНИЙ КЛАС ФУНКЦІОНАЛЬНИХ МАТЕРІАЛІВ.

Ч. 1: Методи виготовлення, структура, фізико-механічні властивості

У статті розглянуто особливий клас конструкційних матеріалів — аморфні сплави. Структурний стан аморфних металевих сплавів (на відміну від кристалічних) характеризується відсутністю трансляційної симетрії в розташуванні атомів і наявністю лише близького атомного порядку. Показано, що основними експериментальними методами підтвердження утворення аморфної структури є рентгенівський фазовий аналіз (XRD) та диференційна сканувальна калориметрія (DSC). Охарактеризовано особливості впливу умов одержання, структурної релаксації та кристалізації на механічні властивості аморфних сплавів. Зазначено наявні відмінності у процесах деформації між кристалічними та аморфними сплавами. Деформація кристалічних сплавів відбувається завдяки ковзанню дислокацій, тоді як у аморфних сплавах цей процес проходить за допомогою локальної атомарної перебудови, тому він і потребує істотно більшої енергії або напруження. Визначено, що залежно від хімічного складу аморфного сплаву можуть бути реалізовані три основні типи реакції кристалізації. Перший тип — поліморфна кристалізація, за якої аморфний сплав без зміни складу переходить у пересичений твердий розчин, метастабільну або стабільну кристалічну фазу. Другий — дві кристалічні фази утворюються одночасно за евтектичним механізмом. Третьому типу відповідає первинна кристалізація, за якої на першій стадії утворюється одна стабільна або метастабільна фаза.

Ключові слова: аморфний сплав, металеве скло, швидкість охолодження, близький атомний порядок, механічні властивості.